11th World Congress on Computational Mechanics (WCCM XI)
5th European Conference on Computational Mechanics (ECCM V)
6th European Conference on Computational Fluid Dynamics (ECFD VI)
E. Oñate, J. Oliver and A. Huerta(Eds)

A NEW METHODOLOGY FOR ESTIMATING CAVITATION EROSION: APPLICATION ON A HIGH SPEED CAVITATION TEST RIG

Phoevos K. Koukouvinis*[1], George Bergeles[2], Manolis Gavaises[3]

School of Engineering and Mathematical Sciences, City University
London Northampton Square, London, EC1V 0HB
[1]Foivos.Koukouvinis.1@city.ac.uk
[2]George.Bergeles.1@city.ac.uk
[3]M.Gavaises@city.ac.uk

Key Words: *Cavitation, High-speed cavitation tunnel, Erosion modelling.*

Summary. In this work a new methodology for the prediction of flow areas of cavitation erosion is presented. The new methodology is a post processing procedure utilizing the results of the flow field solution; it is based on tracking the cavity boundaries in near-wall regions where the material derivative of the vapour volume fraction is reducing, meaning that in these areas the vapour structures are collapsing. Three cavitation erosion indexes are proposed and tested, by simulating the flow formed in a high-speed cavitation tunnel at Laboratoire des Ecoulements Géophysiques et Industriels (LEGI) of the University of Grenoble, where experimental erosion results have been obtained in the past. Agreement between the experimental data and the predictions is satisfactory, indicating the research road for developing an accurate prediction methodology of erosion and material loss.

1 INTRODUCTION

Cavitation occurrence is possible in all hydraulic related systems and machinery, such as piping, valves, pumps, turbines, propellers and others, leading often to lower operating efficiency, reduced flow rates, flow choking, noise, vibration and damage of mechanical components due to material erosion [1]. Thus, in recent years, there has been increased effort for studying cavitation effects, either experimentally or with CFD simulations, aiming to understand the physics of cavitation itself and find a correlation between cavitation occurrence and erosion damage.

Cavitation erosion is not yet well understood and it is a subject of ongoing research. According to Franc et al.[2], erosion due to cavitation may be attributed to the microjet effect, collective bubble collapse and the collapse of cavitating vortices. T.G. Leighton [3] considers the microjet effect dominant when the cavitation intensity is low, whereas in cases of intense cavitation, erosion is predominantly attributed to the shock wave from the collective bubble collapse. Terwisga et al. [4] reviewed the various mechanisms of erosion and concluded that a bubble implosion may trigger the implosion of a bubble cloud leading to cavitation erosion. In any case, the main mechanism that is believed to be the cause of erosion is the localized and focused release of accumulated potential energy in vapour structures, during their collapse. In the recent literature there have been several attempts for modelling erosion effects; a brief, non-exhaustive list includes the works of:

- Li et al. model [5], that is based on time averaged indexes of flow field variables. The conclusion was that the maximum time derivative of pressure in unsteady cavitating flows is a better criterion for cavitation damage, whilst the rate of change of vapour fraction does not correlate with erosion damage.
- Patella et al. [6] proposed a model based on the energy emitted from a collapsing bubble
- Dular et al. model [7], based on the hypothesis that erosion is caused only by microject formation
- Wang et al. model [8], based on bubble dynamic relations along with the pressure wave emissions from collapsing bubble clouds.

In the present work, we propose a methodology for correlating cavitation with erosion. The model is based on the principle that erosion sites appear on surfaces in flow areas where there is vapour bubble collapse due to adverse pressure gradient. As the bubbles near collapse are small they should follow the streaklines of the flow and, therefore, the erosion areas should be topologically defined at least as flow areas where:

$$\left.\begin{aligned}\frac{Da}{Dt} &< 0\\ \frac{Dp}{Dt} &> 0\end{aligned}\right\} \tag{1}$$

where a and p are the vapour volume fraction and the fluid pressure, while D/Dt the total derivative of the flow. Based on the above concept three erosion indexes are proposed and evaluated against experimental data. It has to be noted that the proposed principle for indicating the locations of surface erosion does not depend on the two-phase flow model employed to estimate cavitation; therefore it may be applied in any methodology for calculating cavitating flows, either in an Eulerian or in a Lagrangian framework.

2 EXPERIMENTAL SETUP

The experimental installation consists of a closed flow circuit and is described very well in [9]; it consists of a pump driven by an 80KW electric motor, capable of operating at flow rates of 11lt/s and pressures of 40bar, a heat exchanger to control the temperature of the working fluid (which is water), a flowmeter for the flow measurement, a pressurization bottle

used to adjust the downstream pressure of the device and the test rig. The test section is axis-symmetric and consists of a converging nozzle which accelerates the flow. The flow is then forced to make a 90° turn and to pass between two closely spaced disks, see also Fig. 1.

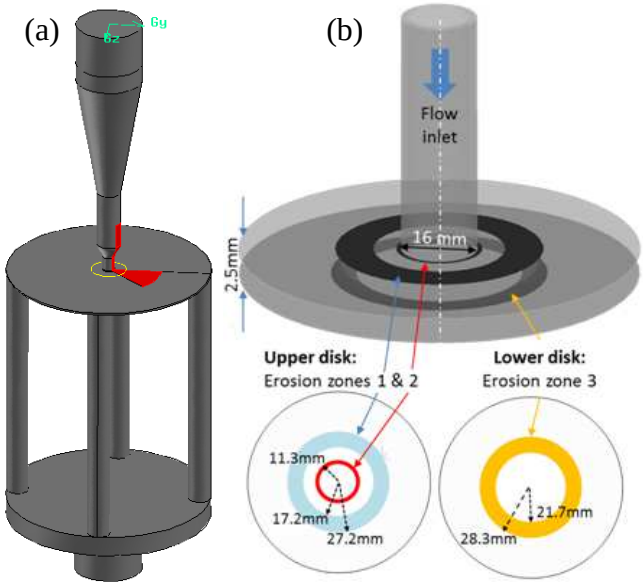

Fig. 1.(a) The experimental test section of the high-speed cavitation tunnel. The computational domain is shown in red. (b) A close-up at the area of interest [9]. The erosion regions are also shown.

The aforementioned installation is primarily used to test material resistance to cavitation erosion. When the device is operating, sheet cavitation is formed just at flow turn, which is convected downstream, causing material erosion to both disks. The lower disk (see Fig. 1) is normally made from a sample material whose erosion resistance is to be determined. The upper disk is made of hardened alloy in order to withstand cavitation erosion and is periodically replaced. Over time, a circular pattern of erosion is formed on the surface of both disks.

3 CFD METHODOLOGY

3.1. Cavitation modeling

The simulations of the flow field for the aforementioned geometry were done using the Fluent v14.5.7 software. For the selection of the appropriate multiphase model, it was kept in mind that, with the current hardware, it is computationally impossible to accurately resolve the dimensions of all cavitation structures, using an interface capturing methodology. Thus, the mixture model [10] was selected, since each computational cell represents a spatially averaged distribution of the vapour/liquid phases, which are assumed to be interpenetrating. Relevant properties, such as density and viscosity, are calculated by volume fraction weighted averaging. Gravity and vapour phase drag force have not been included in the simulation.

The volume fraction of the vapour phase a is calculated by solving an additional scalar

transport equation. Cavitation is handled by mass transfer source terms, which correspond to the evaporation (mass transfer from liquid to vapour) and condensation (mass transfer from vapour to liquid) processes. In this work, these terms are approximated by employing the Zwart-Gerber- Belamri model [10].

3.2. Turbulence modeling

In order to model turbulence effects, the Detached Eddy Simulation model has been used. The Detached Eddy Simulation model is a hybrid between RANS and LES turbulence models [11, 12], which combines the advantages of both methodologies: lower computational cost than pure LES and better representation of vortices and detached eddies the pure RANS, when the grid resolution is fine enough. The RANS part of the DES model is represented using the k-omega SST model, since it is capable of representing near wall flows for y+ less than unity up to y+ of >30 and it is robust and relatively insensitive to the selection of the turbulent characteristics at boundaries [13].

The DES formulation used is the Improved Delayed DES (commonly known as IDDES), since it employs special shielding functions for attached boundary layers and includes the correction of the potential log-layer mismatch [11].

The reasoning behind the selection of this particular turbulence models is twofold:

1. After experimental investigation of the developing flow field between the two disks, it was found that a complicated vortex shedding-like mechanism occurs. Significant vorticity is generated at the sharp turn which is convected downstream, where it decays due to viscosity. Due to the intense vorticity production, pressure at the vortex cores drops below the saturation pressure, thus vortices act like moving cavitation inception sites. It becomes apparent that turbulent effects play a detrimental role at the flow development and, thus, an advanced model is desirable for the correct representation of the flow structures.

2. It has been shown in literature that standard RANS/URANS methodologies fail to predict correctly the vortex generation mechanism in cavitating flows. Here the reader is referred to the works of Coutier Delgosha et al. [14, 15] and Li [5].

4 EROSION MODELING

As mentioned in the introduction, the main idea behind the erosion indexes presented here is the tracking of the collapse of the cavitation vapour structures. In particular, when the vapour structures are collapsing it will be assumed that erosion is produced in the nearby walls, either due to shock wave emission or microjet formation.

Since the simulation is based on an Eulerian reference frame, the collapse of vapour structures will be tracked from the Largangian or material derivative of the vapour volume fraction, *a*, which is defined as:

$$\frac{Da}{Dt} = \frac{\partial a}{\partial t} + \mathbf{u} \cdot \nabla a \tag{2}$$

When the *Da/Dt* term is negative, then the vapour structures are collapsing.

Apart from the material derivative of the vapour/liquid volume fraction, an additional index that has the potential of indicating erosion aggressiveness is the material derivative of pressure, *Dp/Dt*, when the vapour fraction is reducing. The idea behind this index is that the higher the *Dp/Dt* term is, the quicker the collapse of vapour cavities will be; in other words, it quantifies the aggressiveness of the bubble collapse.

An alternative erosion index is the estimation of the number of bubble collapses per volume and time, referred to thereafter as n_{BC}. This rate of bubble collapse may be approximated as follows:

$$\frac{a}{1-a} = nV_b \Rightarrow a = \frac{nV_b}{1+nV_b} \Rightarrow$$

$$\frac{Da}{Dt} = \frac{V_b \dot{n} + nV_b}{\left(1+nV_b\right)^2} \Rightarrow$$

$$\dot{n}_{BC} = n\frac{1}{a(1-a)}\frac{Da}{Dt} - n\frac{\dot{V}_b}{V_b} \tag{3}$$

where n is the number of bubbles per unit volume, V_b is the volume of one bubble. Here, for simplicity, the second term, involving the rate of change of the bubble volume $\dot{V}_b$, is not simulated (is currently under modelling) and will be neglected since under the assumption of sudden collapse at constant bubble radius the term vanishes. As the collapsing bubbles have almost the same potential energy [16], this index is proportional to the energy release per unit time and volume.

Finally, an alternative measure of the cavitation erosion potential is the acoustic pressure, p_{ac}, emitted during the bubble collapse phase. This may be approximated, beginning from the following relation of Wang and Brennen [8]:

$$p_{ac} = \frac{\rho}{4\pi r}\frac{D^2 V_B}{Dt^2}$$

since $V_B = V_C a$

$$p_{ac} = V_C \frac{\rho}{4\pi r}\frac{D^2 a}{Dt^2} \tag{4}$$

where V_c is the local cell volume, ρ is the fluid density, r is the distance from the wall. It should be highlighted here, that in both the rate of the number of bubble collapses and the acoustic pressure, only positive values have a practical meaning for erosion.

5 CFD SIMULATION RESULTS

5.1. Instantaneous and mean flow results

In order to simplify the simulation and decrease the computational cost, due to spatial and temporal resolution requirements of the turbulence model used, only 1/8th of the complete axis-symmetric geometry was simulated (see also Fig. 1). The computational mesh employed

is purely hexahedral, non-conformal, consisting of ~5 million cells. Adaptive refinement is used near the area of interest, which spans between 0 and 35mm, including the erosion zones of both upper and lower disks. The boundary conditions used are shown in Fig. 2; the flow rate through the device is prescribed to 8.16lt/s, which corresponds to an inlet velocity of 9.66m/s, while the absolute pressure at the outlet is set to 19bar. The saturation pressure of water is set to 2340Pa, which corresponds to a temperature of 20°C. From the experiment at these conditions, the absolute pressure at the inlet is found to be ~40bar and the test rig is operating at a cavitation number σ of 0.9.

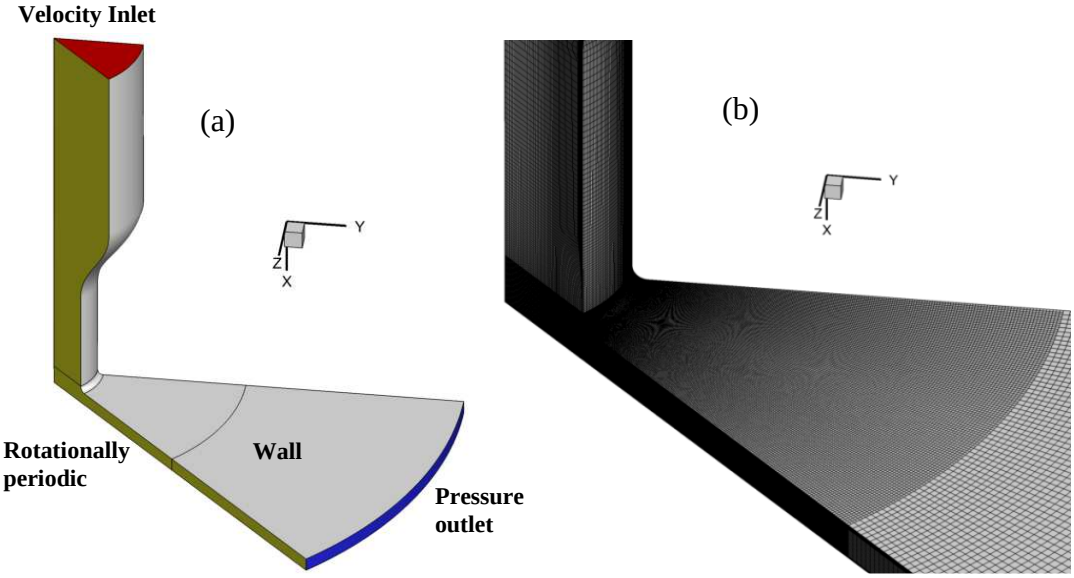

Fig. 2.(a) boundary conditions used for the simulation (b) computational mesh used, with refinement visible

The spatial resolution used is ~0.1mm and at the area of refinement is ~0.05mm. Refinement is used at the near wall region in order to capture as much as possible the near wall effects and the flow detachment; indicatively, the first near wall cell at the sharp turn had a height of 2.5μm. The temporal resolution used is 2μs. The idea behind the selection of this time step was based on the fact that, with DES, one may resolve eddies with maximum wavelength of $\lambda=5\Delta$, where Δ is the average mesh resolution [17]. Thus, this corresponds to indicative length scale of ~0.5mm and, when considering a maximum velocity of 90m/s which occurs at the turn, results to a time scale of 2.7μs.

Indicative instantaneous results are shown in the following figures. In Fig. 3 the vortical structures after the sharp turn are shown using (a) the second invariant of the velocity gradient tensor and (b) the vorticity magnitude. The reason for using the second invariant of the velocity gradient is because it represents in a better way the vortical structures than vorticity itself (the interested reader is addressed to e.g. [12, 18, 19]); vorticity is high not only in vortices, but in areas of high shear as well, thus masking the actual vortices [19]. From Fig. 3 it becomes apparent that there is significant vortex generation downstream the turn.

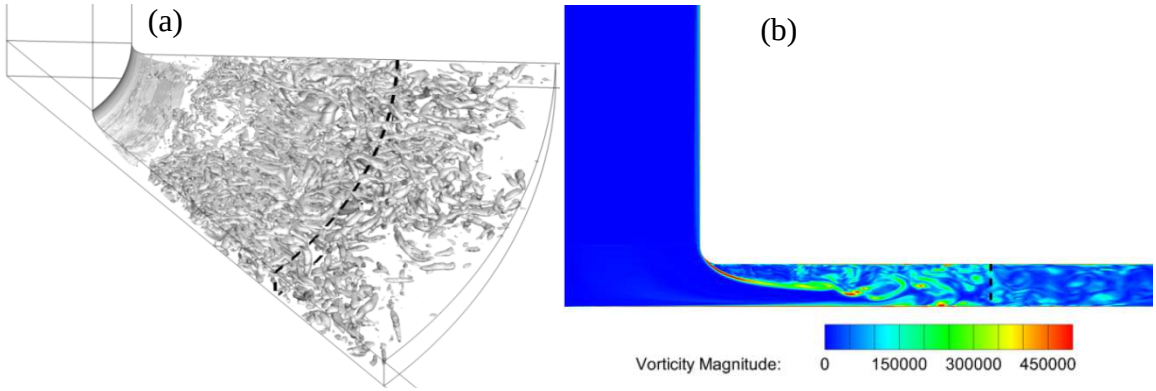

Fig. 3. (a) Isosurface of the velocity gradient second invariant. (b) Contour of vorticity magnitude. The black dashed line shows the radius of 25mm.

The simulation was run for 0.0125s of physical time, while statistics have been collected for 5ms. In Fig. 4, the distribution of the instantaneous and averaged liquid phase fraction is shown. The instantaneous vapour distribution is highly irregular and unsteady. On the other hand, the averaged distribution of the phase fraction shows a smooth transition, with vapour generation being intense near the turn and fading out when moving closer to the radius of 25mm.

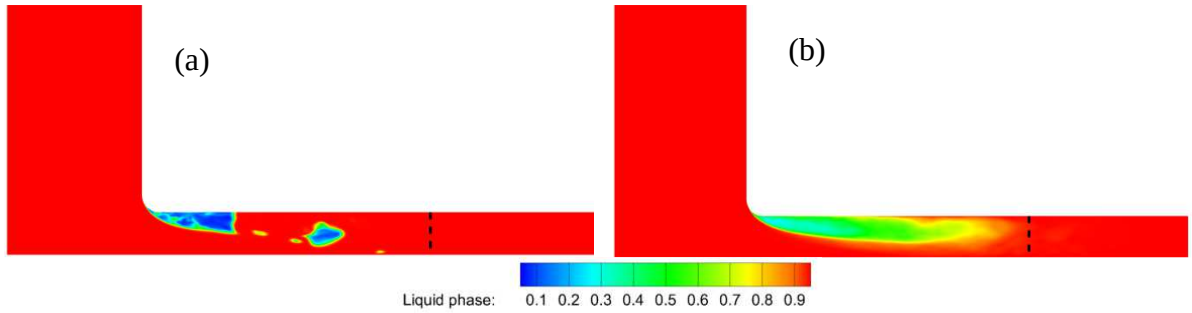

Fig. 4. (a) Instantaneous and (b) averaged liquid phase fraction. The black dashed line shows the radius of 25mm.

5.2. Erosion indexes

The statistics of the liquid fraction may be used as an equivalent steady-state solution field which shall be used for the derivation of the erosion indexes on the wall surfaces; in that case, the temporal term of eq. 2 is dropped out. In the following figures (Fig. 5 - Fig. 8) results from the erosion indexes are shown, in comparison with the actual erosion sites found from the experiments (dashed lines, see Fig. 1).

The maximum values of the total derivative of the vapour volume fraction, shown in Fig. 5 marginally approach the lower edge of the erosion areas in both disks. The total derivative pressure however, D*p/Dt*, index shows a different pattern: the maximum values fall inside the erode areas. Predicted erosion on the upper disk is limited to a rather narrow zone inside the

actual erosion zone at R=17.2 - 27.2mm; the rest of the upper disk is practically predicted free of erosion. On the other hand, at the lower disk very high values are predicted near R = 21.7mm, in agreement with the experimental evidence. The n_{bc} index shown in Fig. 7 are correlated better with the experimental evidence regarding the location and extent of the eroded areas. Fig. 8 present the erosion index based on the values of the emitted acoustic pressure upon vapour collapse; high erosion values are predicted earlier comparing with the experiment at the lower disk, whilst the index predicts rather successfully the erosion situation in the upper disk.

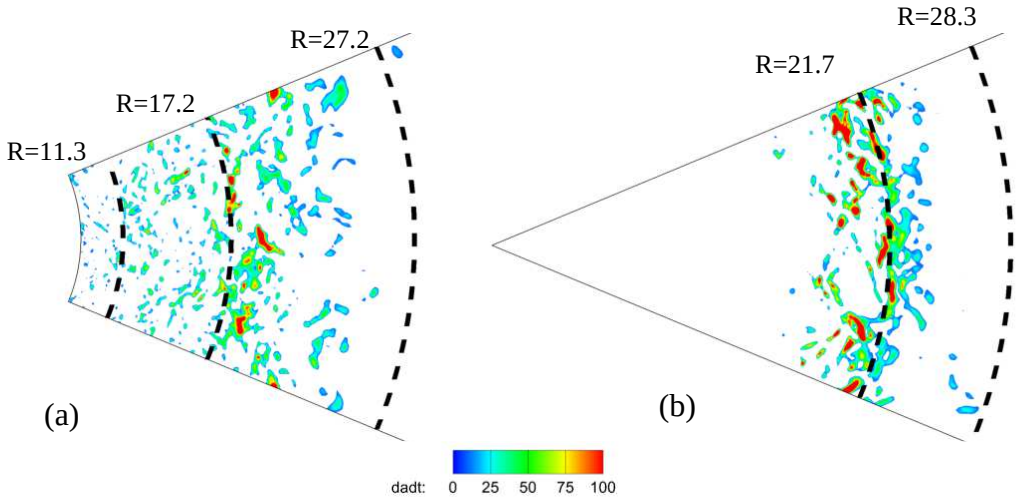

Fig. 5. Volume fraction material derivative at (a) upper and (b) lower disks.

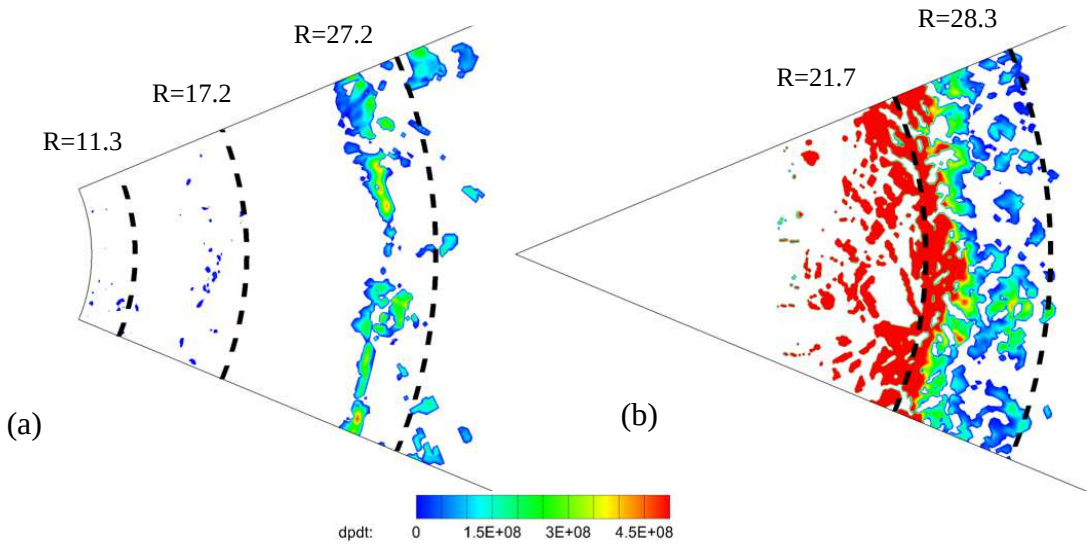

Fig. 6. Pressure material derivative (*Dp/Dt*) in near wall areas where the vapour structures are collapsing (*Da/Dt<0*), at the (a) upper and (b) lower disk.

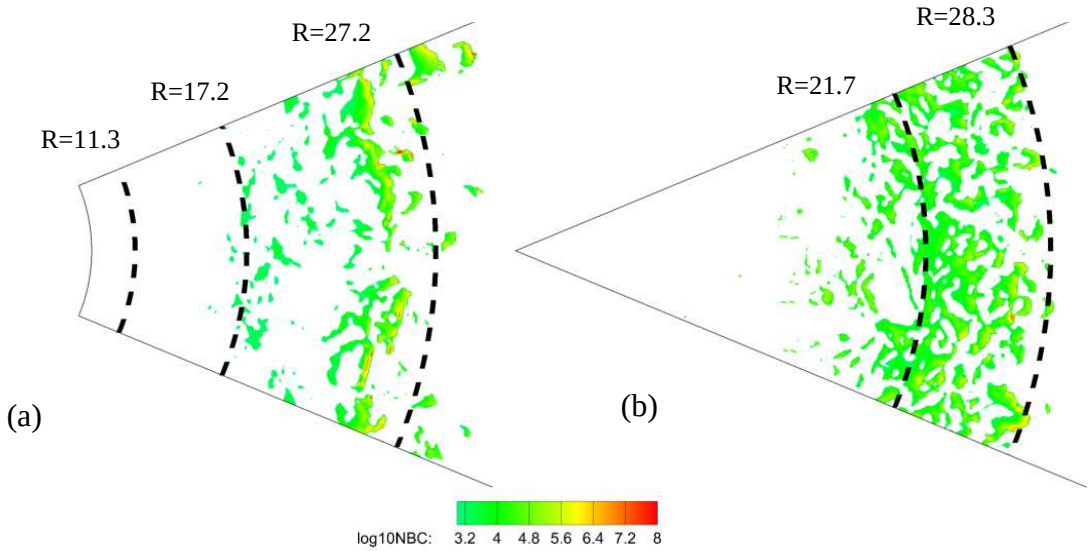

Fig. 7. Number of bubbles collapsing (n_{BC}) near the wall at the (a) upper and (b) lower disk. Note that the decimal logarithm is plotted.

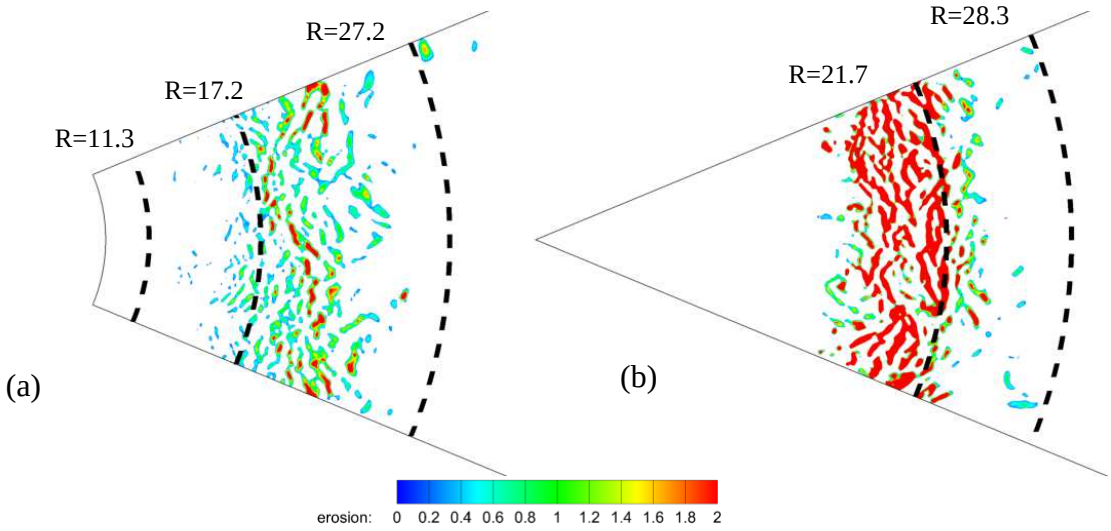

Fig. 8. Erosive pressure (p_{ac}) calculated from the second material derivative of the liquid volume fraction at the (a) upper and (b) lower disk.

Considering all results from the new erosion models, some conclusions can be drawn:

- The predicted potential sites for erosion based on the proposed indexes are close to the actual pattern observed from the experiments, with the rate of the number of bubble collapse index to be the superior. There are of course discrepancies, which are examined at the next points.
- Erosion at both the upper and the lower disk is predicted somewhat earlier than the actual

erosion of the experiment. Indeed, all methodologies predict high erosion indexes near the lower radius of the erosion zones of R= 17.2-27.2mm and R= 21.7 - 28.3mm of the upper and lower disk respectively. This is believed to be caused by a general underestimation of the extension of the vapour phase; this is also visible in Fig. 4 where the vapour phase has practically collapsed after a radius of ~23mm. It also seems that this effect is not related to the flow field resolution, since a mesh dependence study was performed and the average value of the vapour field did not vary significantly. So, it could be the case that the semi-empirical cavitation model, employed in Fluent, and in particular the vapour condensation parameter, requires tuning, in order to properly capture the correct cavity size and location of the vapour collapse.

- Erosion at the upper disk at the zone of 9-11.3mm was not captured by any erosion model. It is expected that this particular zone would be hard to capture, since it is close to the flow detachment point and the flow field there is rather complicated and highly unsteady.

6 CONCLUSION

In the current work, three erosion indexes have been tested for estimating areas of potential cavitation damage. The Erosion Indexes are based on the tracking of the vapour structures collapse; in practice, material derivatives of the vapour fraction and pressure field are employed. The described methodology is applied to the unsteady, turbulent, cavitating flow field inside a high speed cavitation tunnel, since extensive data of the erosive pattern are published. The flow field has been resolved and time averaged values of the velocity, pressure and vapour phase fields have been extracted, which have then been used for the calculation of the proposed erosion indexes. Generally, the predicted erosion areas are similar to the experimentally found pattern, with the rate of the number of bubble collapse erosion index to show superior performance. Discrepancies which are found are attributed mainly to the cavitation model used, as the size of the cavity evolution is not accurately captured.

ACKNOWLEDGEMENTS

The authors would like to acknowledge the contribution of The Lloyd’s Register Foundation. Lloyd’s Register Foundation helps to protect life and property by supporting engineering-related education, public engagement and the application of research. The research leading to these results has also received funding from the People Programme (Marie Curie Actions) of the European Union's Seventh Framework Programme FP7/2007-2013/ under REA grant agreement n. 324313.

REFERENCES

[1] J. P. Tullis and B. P. Tullis, "The CRC Handbook of Mechanical Engineering, Second Edition," in *Handbook Series for Mechanical Engineering* F. Reith and Y. Goswami, Eds., 2nd ed, 2004.

[2] J.-P. Franc and J.-M. Michel, *Fundamentals of Cavitation*: Springer, 2004.

[3] T. G. Leighton, *The acoustic bubble*: Academic Press 1994.

[4] Z. R. Li, M. Pourquie, and T. Terwisga, "A numerical study of steady and unsteady cavitation on a 2d hydrofoil. Journal of Hydrodynamics," *Journal of Hydrodynamics* vol. 22, 2010.
[5] Z. R. Li, "Assessment of cavitation erosion with a multiphase Reynolds-Averaged Navier-Stokes method," PhD Thesis, TU Delft, 2012.
[6] R. F. Patella, A. Archer, and C. Flageul, "Numerical and experimental investigations on cavitation erosion," presented at the 26th IAHR Symposium on Hydraulic Machinery and Systems, 2012.
[7] M. Dular and O. Coutier-Delgosha, "Numerical modelling of cavitation erosion," *International Journal for Numerical Methods in Fluids,* vol. 61, pp. 1388-1410, 2009.
[8] Y. C. Wang and C. E. Brennen, "Numerical Computation of Shock Waves in a Spherical Cloud of Cavitation Bubbles," *Journal of Fluids Engineering,* vol. 121, pp. 872-880, 1999.
[9] J. P. Franc, M. Riondet, A. Karimi, and G. L. Chahine, "Material and velocity effects on cavitation erosion pitting," *Wear,* vol. 274– 275, pp. 248– 259, 2012.
[10] *ANSYS Fluent 14.5.7 manual.*
[11] C. Mockett, *A comprehensive study of detached-eddy simulation*: TU Berlin Universitätsbibliothek 2007.
[12] X. Jiang and C. H. Lai, *Numerical Techniques for Direct and Large-Eddy Simulations* Chapman & Hall/CRC 2009.
[13] H. Versteeg and W. Malalasekera, *An Introduction to Computational Fluid Dynamics: the Finite Volume method*, 2nd ed.: Prentice Hall, 2007.
[14] O. Coutier-Delgosha, J. L. Reboud, and Y. Delannoy, "Numerical simulation of the unsteady behaviour of cavitating flows," *International Journal for Numerical Methods in Fluids,* vol. 42, pp. 527-548, 2003.
[15] O. Coutier-Delgosha, J. L. Reboud, and R. Fortes-Patella, "Evaluation of the Turbulence Model Influence on the Numerical Simulations of Unsteady Cavitation," *Journal of Fluids Engineering,* vol. 125, pp. 38-45, 2003.
[16] C. E. Brennen, *Cavitation and Bubble Dynamics*: Oxford University Press, 1995.
[17] P. R. Spalart and C. Streett, "Young-Person's Guide to Detached-Eddy Simulation Grids," NASA Technical Report 2001.
[18] C. Silva and J. Pereira, "Invariants of the velocity-gradient, rate-of-strain, and rate-of-rotation tensors across the turbulent/nonturbulent interface in jets," *Physics of fluids,* vol. 20, 2008.
[19] B. Huang, Y. Zhao, and G. Wang, "Large Eddy Simulation of turbulent vortex-cavitation interactions in transient sheet/cloud cavitating flows," *Computers & Fluids,* vol. 92, pp. 113-124, 3/20/ 2014.